*American Mineralogist, Volume 99, pages 704–711, 2014*

# Solid solutions and phase transitions in $(Ca,M^{2+})M^{2+}Si_2O_6$ pyroxenes ($M^{2+}$ = Co, Fe, Mg)

**Luciana Mantovani[1,*], Mario Tribaudino[1], Giovanni Bertoni[2], Giancarlo Salviati[2] and Geoffrey Bromiley[3]**

[1]Dipartimento di Fisica e Scienze della Terra "Macedonio Melloni," Parco Area delle Scienze 157/A, 43124 Parma, Italy
[2]IMEM–CNR, Istituto dei Materiali per l'Elettronica e il Magnetismo, Parco Area delle Scienze 37/A, 43124 Parma, Italy
[3]School of GeoSciences and Centre for Science at Extreme Conditions, University of Edinburgh, Grant Institute, West Mains Road, Edinburgh EH9 3JW, U.K.

## Abstract

The effect of the substitution of Ca with Co, on the phase transition and on the extension of the miscibility gap, was studied to model the general mechanism of phase transitions and solid solutions in $(Ca,M^{2+})M^{2+}Si_2O_6$ pyroxenes. Eleven pyroxenes with composition $Ca_{1-x}Co_{1+x}Si_2O_6$, $(0 \leq x \leq 1)$ were therefore synthesized by piston cylinder at $P = 3$ GPa, and $T$ between 1100 and 1350 °C. The samples were characterized by SEM-EDS, XRD powder diffraction, and TEM. The results were compared with those of Ca-Fe and Ca-Mg pyroxenes. The phase diagram of Ca-Co pyroxenes is similar to that of Ca-Fe and Ca-Mg ones, with a wide asymmetric miscibility gap, and higher solubility in the Ca-rich side of the gap. The solubility on the Ca-rich side of the gap is related to the radius of the cation substituting.

The cell parameters of the Ca-Co pyroxenes undergo a sudden change at the composition of about 0.4 Ca apfu, due to the $C2/c$–$P2_1/c$ phase transition. The change in volume with composition follows an ideal trend, in the $C2/c$ phase, dictated by the ionic size of the substituting cation. Deviation from the $C2/c$ behavior are instead observed in the $P2_1/c$ field and ascribed to volume strain. The same turnover was found in Ca-Mg, Ca-Fe, and Ca-Mn pyroxenes. The $C2/c$–$P2_1/c$ transition occurs with decreasing the M2 average cation radius, down to a critical value between 0.85 and 0.88 Å, depending on the series. A stabilization of the $C2/c$ phase related to crystal field in Ca-Fe and Ca-Co pyroxenes is suggested by the analysis of the volume strain in the $P2_1/c$ field. A key finding is that a miscibility gap may develop either by lattice strain related to cation substitution, within a series where all end-members have the same structure, or for the combined effect of lattice strain and a phase transition, as is the case for pyroxenes.

**Keywords:** Ca-Co pyroxenes, high-pressure synthesis, phase transition, phase equilibria

## Introduction

One of the most intriguing features of the pyroxene mineral family is the wide range of chemical substitutions, in a relatively simple structure (Redhammer and Roth 2004; Yang and Prewitt 2000). This can be appropriately studied in synthetic pyroxenes, which provide a structural model to interpret the behavior of natural pyroxenes with temperature, pressure, and composition. Synthetic pyroxenes, therefore, have been the subject of extensive investigation (Tribaudino 2000; Tribaudino and Nestola 2002; Redhammer et al. 2012; Downs 2003), to detail the flexibility of the pyroxene structure, to show new phase transitions, the effect of crystal chemical substitutions on such transitions and, for pyroxenes bearing transition elements, the effect of structural changes on the electronic transitions. More recently the properties of transition metal-bearing synthetic pyroxenes were widely investigated in view of the discovery of multiferroic behavior in pyroxenes (Jodlauk et al. 2007; Redhammer et al. 2011a, 2011b).

Among transition metals, $Co^{2+}$ is able to enter the pyroxene structure in the M1 site within the little distorted M1 octahedron, and in the M2 sixfold- to eightfold-coordinated site.

Most studies on Co pyroxenes were done on monoclinic $CaCoSi_2O_6$ (Navrotsky and Coons 1976; Ghose et al. 1987) and orthorhombic $Co_2Si_2O_6$ (Akimoto et al. 1965; Sasaki et al. 1982) end-members. Moreover the magnetic properties of end-member Ca-Co pyroxenes at low temperature (Durand et al. 1996; Redhammer et al. 2008), and the visible absorption spectrum (White et al. 1971; Burns 1993), were also studied. Intermediate cobalt pyroxenes, which can be represented in the series $CaCoSi_2O_6$–$Co_2Si_2O_6$, were only studied in the recent single crystal structural investigation (Mantovani et al. 2013). In such solid solution Co fills the M1 site, and the substitution along the series occurs between Ca and Co in the M2 site. The ionic radius of Co is intermediate between that of Mg and Fe (0.745 vs. 0.72 and 0.78 Å, respectively) (Shannon 1976) and the crystal chemistry of $(Ca,Co)CoSi_2O_6$ pyroxenes is expected to be similar to that of quadrilateral pyroxenes diopside-enstatite (Di-En, $CaMgSi_2O_6$-$Mg_2Si_2O_6$, hereafter Ca-Mg pyroxenes) and hedenbergite-ferrosilite (Hd-Fs, $CaFeSi_2O_6$-$Fe_2Si_2O_6$, hereafter Ca-Fe pyroxenes). These series share the point that chemical changes occur only for the substitution of Mg, Fe, Co for Ca, i.e., smaller for a bigger cation, in the M2 site.

* E-mail: luciana.mantovani@unipr.it

0003-004X/14/0004–704$05.00/DOI: http://dx.doi.org/10.2138/am.2014.4684

At room pressure the only Ca-Co pyroxene phase that can be synthesized is the end-member $CaCoSi_2O_6$; further Co addition results in the formation of olivine and silica (Mukhopadhyay and Jacob 1987). At high pressure, $P > 3$ GPa, the orthorhombic and monoclinic $Co_2Si_2O_6$ phases were obtained by Akimoto et al. (1965), but no other systematic study at high pressure was performed on Co pyroxenes. Phase equilibria in Ca-Co pyroxenes are similar to those in the Ca-Fe pyroxenes that at room pressure crystallize incongruently fayalite and quartz, whereas at high pressure the pyroxene phases are stable through the join.

In Ca-Mg and Ca-Fe pyroxenes, the space group at room conditions changes from $C2/c$ to $P2_1/c$ and then to $Pbca$, as Ca content decreases; orthorhombic pyroxenes are confined to the Ca-poorer composition, whereas the transition from $C2/c$ to $P2_1/c$ occurs at a Ca content of ~0.3 and ~0.6 apfu, respectively, in Ca-Fe (Ohashi et al. 1975) and in Ca-Mg pyroxenes (Newton et al. 1979; Tribaudino 2000; Tribaudino et al. 2005). It was proposed that the $C2/c$ to $P2_1/c$ phase transition occurs as the average cation radius in the M2 site becomes lower than the critical value of 0.88 Å (Arlt et al. 1998).

Moreover, in both Ca-Mg and Ca-Fe pyroxenes, there is a miscibility gap between Ca-rich and Ca-poor compositions. It is asymmetric, with higher solubility on the Ca-richer limb, and widens with increasing pressure; also, it is larger in Ca-Mg pyroxenes (Gasparik and Lindsley 1980; Lindsley and Munoz 1969).

We expect that the same transition and miscibility gap also occurs in Ca-Co pyroxenes; a comparison with Ca-Fe and Ca-Mg ones can provide the basis of a model of solid solutions in pyroxenes.

In this work, a series of $(Ca,Co)CoSi_2O_6$ pyroxenes was synthesized at high pressure, and analyzed by XRD, SEM-EDS, and TEM, to clarify the extension of the solid solutions and the symmetry changes along the series. The results were compared with those of Ca-Fe and Ca-Mg pyroxenes to model the effect of the substitution of Ca with a smaller cation, on the phase transition and on the extension of the miscibility gap.

Single-crystal refinements of $C2/c$ Ca-Co pyroxenes synthesized in the present study have been instead reported in a previous paper (Mantovani et al. 2013).

## Experimental methods

### Synthesis

The starting materials for the high-pressure experiments were obtained by annealing high-grade reagents of amorphous $SiO_2$ (Sigma-Aldrich 99.995%), $CaCO_3$ (Sigma-Aldrich 99.995%), and $Co_3O_4$ (Sigma Aldrich >99.99%). The stoichiometric mixtures were prepared to obtain the composition of $Ca_xCo_{1-x}CoSi_2O_6$ pyroxenes, with x varying from 0 to 1 at step of 0.1 Ca apfu (Table 1). Slight silica excess (about 1–2 wt%) was present in all samples to avoid the formation of silica subsaturated phases. At first the samples were annealed at $P = 1$ atm and $T = 1000$ °C for 12 h; XRD analysis of the annealed samples showed almost pure $CaCoSi_2O_6$ pyroxene, Co-akermanite ($Ca_2CoSi_2O_6$), and Co-olivine ($Co_2SiO_4$), in various amounts depending on the Co content and, in all samples, an excess of $SiO_2$ in the form of trydimite, cristobalite, and amorphous silica. The mixture, after fine grinding, was used for the high-pressure experiments. A ½ inch piston-cylinder apparatus and a pyrex-talc assembly containing an internal graphite furnace was used (Bromiley et al. 2004), and the experiments were run at $P = 3$ GPa and in a $T$ range between 1100 and 1350 °C. Pressure and temperature were maintained at this condition from 1 to 7 h after which the heating system was switched off and the samples quenched. Temperature was measured with a Pt-Pt10%Rh thermocouple. A small amount of water was added to enhance reaction. The experimental conditions are reported in Table 1.

Run products were at first analyzed optically. They appeared as a tiny pink bunches of crystals of the order of tens of micrometers in length (Fig. 1). Sharp optical extinction was noted.

### SEM-EDS and X-ray powder diffraction

A few grains of the run products were embedded in epoxy and polished for SEM-EDS analysis using a Jeol 6400 SEM equipped with an Oxford EDS, operated at 20 kV. Electron backscattered images were taken on the same area where the microprobe analysis was performed. The crystals are euhedral and compositionally homogeneous (Fig. 2).

At least 10 analytical spots were collected in each run product. The average results of the chemical analyses were expressed in atoms per formula unit, calculated on the basis of six oxygen and four cations and reported in Table 1; the standard deviation is reported in parentheses, and it is calculated on the average of 10 analytical spots.

From the remaining sample powder diffraction was conducted using a Bruker-AXS D8 Advance and Cu$K\alpha$ radiation ($\lambda = 1.54178$ Å). Intensity measurements were taken in steps of 0.02° over 2θ range from 10 to 80°, with a counting rate of 1.3 s per step. Rietveld analysis was performed to determine the unit-cell parameters and quantify the phases present. GSAS-EXPGUI software package was used (Larson and Von Dreele 1994; Toby 2001). Starting atomic parameters were taken from Ghose et al. (1987) for $C2/c$, and from Sasaki et al. (1982) for $Pbca$ pyroxenes. For $P2_1/c$ pyroxenes, the atomic parameters are taken from the structure of clinoferrosilite (Hugh-Jones et al. 1994), but with the substitution of the iron atoms with cobalt. The site occupancy of the intermediate pyroxenes was derived by the EDS results. The cell parameters and phase fractions are reported in Table 1.

**Table 1.** Synthesis condition, chemical analyses, and cell parameters of the synthetized samples

| Sample | Nominal Ca (apfu) | $P$ (GPa) | $T$ (°C) | Time (h) | Ca (apfu) | Co (apfu) | Si (apfu) | Phase | $a$ (Å) | $b$ (Å) | $c$ (Å) | β (°) | $V$ (Å³) |
|---|---|---|---|---|---|---|---|---|---|---|---|---|---|
| Co0 | 1 | 3 | 1200 | 6 | 0.997(11) | 0.968(14) | 2.023(10) | cpx | 9.802(1) | 8.962(1) | 5.249(1) | 105.40(1) | 444.54(3) |
| Co1 | 0.9 | 3 | 1200 | 4 | 0.949(8) | 1.058(7) | 1.995(8) | cpx | 9.799(1) | 8.949(1) | 5.246(1) | 105.53(1) | 442.81(3) |
| Co2 | 0.8 | 3 | 1200 | 6 | 0.860(8) | 1.133(6) | 2.005(5) | cpx | 9.791(1) | 8.954(1) | 5.246(1) | 105.77(1) | 442.58(8) |
| Co3 | 0.7 | 3 | 1200 | 4 | 0.723(15) | 1.283(17) | 2.010(6) | cpx | 9.777(1) | 8.958(1) | 5.242(1) | 106.13(1) | 441.05(8) |
| Co4 | 0.6 | 3 | 1200 | 4 | 0.618(19) | 1.397(31) | 2.005(13) | cpx | 9.769(1) | 8.964(1) | 5.243(1) | 106.46(1) | 440.28(3) |
| Co5 | 0.5 | 3 | 1100 | 5 | 0.687(30) | 1.319(32) | 1.997(7) | cpx (65.3%) | 9.798(1) | 8.984(1) | 5.258(1) | 106.33(1) | 445.21(1) |
| | | | | | 0.106(51) | 1.897(48) | 2.007(11) | + opx (34.6%) | 18.357(2) | 8.941(1) | 5.224(1) | | 857.3(1) |
| Co5 | 0.5 | 3 | 1280 | 5 | 0.519(28) | 1.488(33) | 2.009(6) | cpx | 9.751(1) | 8.962(1) | 5.239(1) | 106.78(1) | 438.28(9) |
| Co5 | 0.5 | 3 | 1350 | 6 | 0.517(14) | 1.498(5) | 2.018(23) | cpx | 9.753(1) | 8.964(1) | 5.238(1) | 106.83(1) | 438.41(8) |
| Co6 | 0.4 | 3 | 1200 | 6 | 0.626(35) | 1.376(36) | 1.999(5) | cpx (66.6%) + | 9.747(1) | 8.955(1) | 5.233(1) | 106.64(1) | 437.66(5) |
| | | | | | 0.110(11) | 1.891(17) | 2.000(5) | opx (33.3%) | 18.338(3) | 8.927(2) | 5.207(1) | | 852.48(9) |
| Co6 | 0.4 | 3 | 1350 | 5 | 0.419(23) | 1.596(25) | 1.991(15) | cpx | 9.749(1) | 8.963(1) | 5.237(1) | 106.82(7) | 438.11(9) |
| Co7 | 0.3 | 3 | 1350 | 7 | 0.300(27) | 1.691(19) | 2.010(6) | cpx | 9.717(1) | 8.952(1) | 5.245(1) | 107.92(6) | 434.09(8) |
| Co8 | 0.2 | 3 | 1350 | 4 | 0.209(12) | 1.802(15) | 2.002(4) | pig | 9.707(1) | 8.950(2) | 5.238(1) | 108.43(5) | 431.7(1) |
| Co10 | 0 | 3 | 1200 | 6 | – | 2.012(123) | 2.005(15) | opx | 18.298(2) | 8.921(2) | 5.203(1) | | 849.4(1) |
| Co10 | 0 | 7 | 1000 | 1 | – | 2 | 2 | cpx | 9.650(5) | 8.929(5) | 5.222(3) | 108.8(1) | 424.3(3) |

*Note:* Phase percentage in the two phase assemblage are wt%, determined by Rietveld refinement.

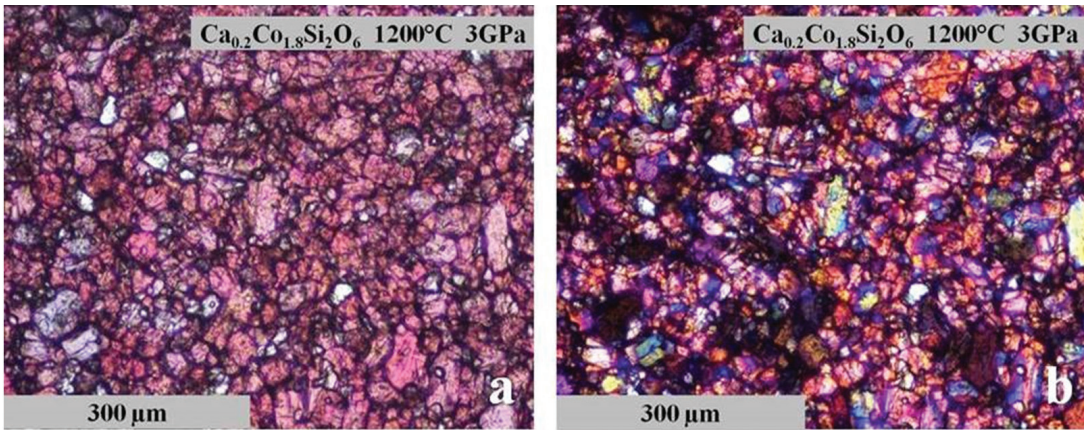


**FIGURE 1.** Images of Ca-Co pyroxenes recorded by optical microscope. (**a**) Parallel polars. (**b**) Crossed polars. (Color online.)

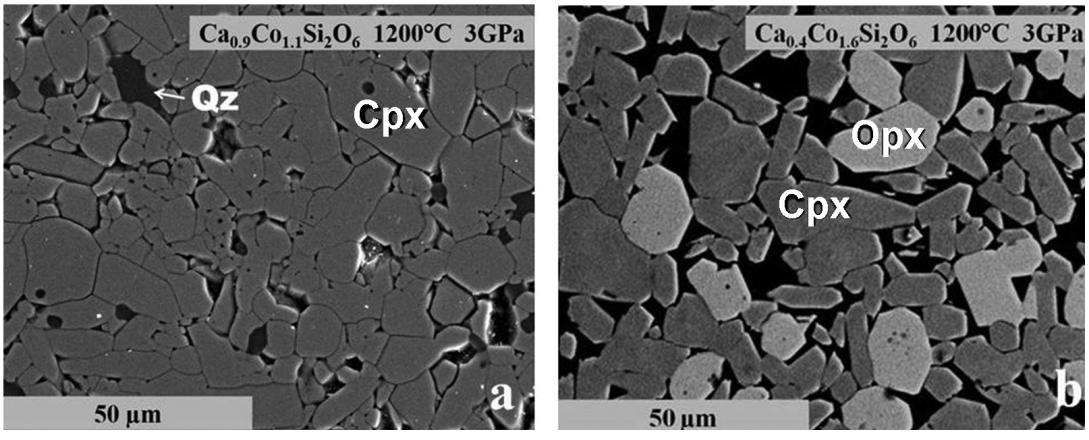


**FIGURE 2.** Backscattered electron images. (**a**) Single clinopyroxene phase in the sample $Ca_{0.9}Co_{1.1}Si_2O_6$. The presence of quartz is related to the excess silica in the starting materials. (**b**) Coexistence of Ca-rich (Cpx) and Ca-poor (Opx) phases in samples $Ca_{0.4}Co_{1.6}Si_2O_6$ (Co6, $T$ = 1200 °C).

### TEM observation

A sample with composition $Ca_{0.3}Co_{1.7}Si_2O_6$, labeled as Co7 in Table 1, was examined by transmission electron microscopy. The sample was crushed, suspended on ispropylic alcohol, and deposited on a holey carbon film. A JEOL JEM-2200FS field emission electron microscope operating at 200 kV equipped with double tilt holder was used. Selected area diffraction patterns were collected along zone axes at different orientation, to show the changes in lattice symmetry.

## RESULTS

### Single and two-pyroxene stability field

SEM-EDS and XRD powder diffraction analysis showed in most runs a single pyroxene phase, with composition very close to the expected pyroxene stoichiometry (Table 1), coexisting with a slight amount of excess quartz related to the excess silica in the starting materials. In a few runs, a two-pyroxene assemblage of Ca-rich and Ca-poor pyroxenes was found (Fig. 2). This happened in syntheses at or below 1200 °C, for starting materials with less Ca than 0.5 apfu in the nominal pyroxene (Lindsley and Munoz 1969; Gasparik and Lindsley 1980).

The coexistence of Ca-poor and Ca-rich pyroxenes was interpreted, in accordance to previous findings for Ca-Fe and Ca-Mg pyroxenes, as evidence of a miscibility gap between pyroxenes.

At 1350 °C the Ca-Co in pyroxene solubility is almost complete, although it is likely that by similarity with Ca-Mg and Ca-Fe phase diagrams, between $Ca_{0.1}Co_{1.9}Si_2O_6$ and $Ca_{0.2}Co_{1.8}Si_2O_6$ a narrow miscibility gap between clino- and orthopyroxenes exists also at 1350 °C.

At 1280 °C no evidence of exsolution for $Ca_{0.5}Co_{1.5}Si_2O_6$ was obtained, whereas at 1200 and 1100 °C a clino–orthopyroxene gap was present. Also, in the TEM observation on $Ca_{0.3}Co_{1.7}Si_2O_6$ at 1350 °C exsolution lamellae of Ca-poorer (or-richer) phases, like those reported in Domeneghetti et al. (1995) and Tribaudino et al. (2003a) were not observed.

The composition of coexisting pyroxenes and of solid solutions reported in Table 1 and the analogy with other pyroxenes allows to sketch the phase diagram between 1100 and 1350 °C (Fig. 3a).

The sketch of the diagram of Ca-Co pyroxenes is compared with that of Ca-Mg and Ca-Fe pyroxenes at $P$ = 3 GPa (Lindsley and Munoz 1969; Gasparik and Lindsley 1980) (Fig. 3b). Most apparent is that the pyroxene solubility decreases on the Ca-rich side with the substituting cation at the M2 site, from Fe to Co and Mg. At about Ca content of 0.5 apfu a single clinopyroxene phase is present at $P$ = 3 GPa between melting and a temperature of 1500 °C for Ca-Mg, 1280 °C for Ca-Co, and 900 °C for Ca-Fe pyroxenes.

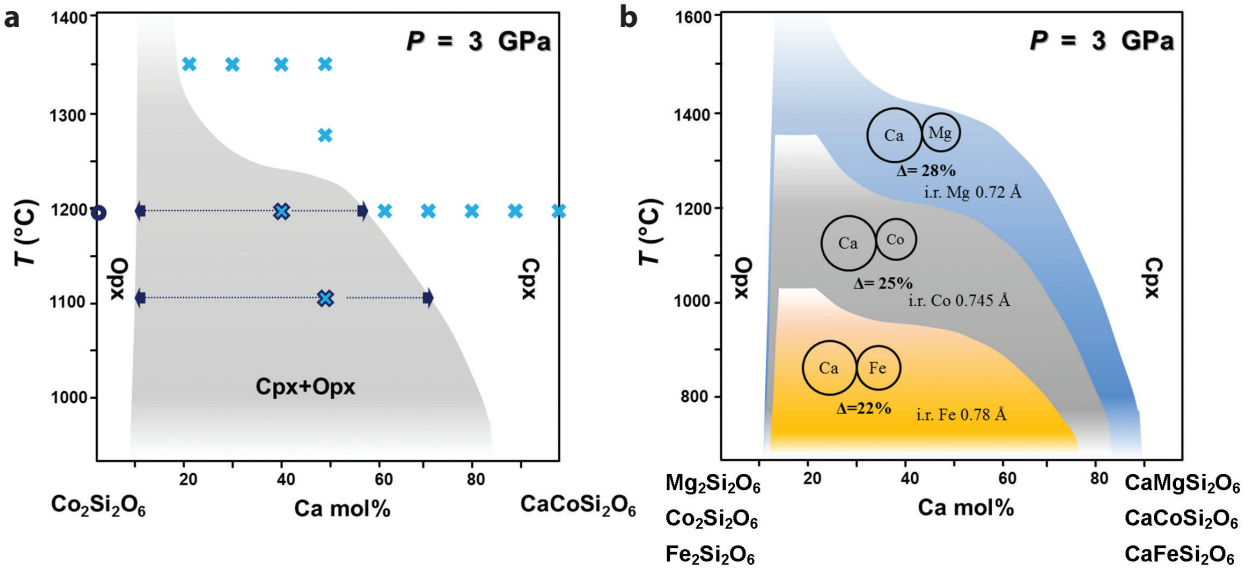


**FIGURE 3.** (**a**) Sketch of a phase diagram of the join $CaCoSi_2O_6$-$Co_2Si_2O_6$ at $P$ = 3 GPa. Light blue crosses represent the monoclinic single phase while deep blue circles the orthorombic phase. Crosses into the miscibility gap represent the cohexistence of Opx and Cpx. The shape of the miscibility gap is built up with reference to literature data for the Ca-Mg and Ca-Fe pyroxene, and it is only loosely constrained by the synthesis experiments. (**b**) Sketch of a comparison at $P$ = 3 GPa between phase diagrams of Ca-Mg (Gasparik and Lindsley 1980), Ca-Fe (Lindsley and Munoz 1969), and Ca-Co pyroxenes (this work); comparative size of Ca and $Fe^{2+}$, Mg and Co ions and ionic radius difference (Δ) are shown. (Color online.)

### Cell parameters, TEM observations, and the $C2/c$–$P2_1/c$ phase transition

The cell parameters of Ca-Co clinopyroxenes are shown as a function of composition in Figure 4. Axial parameters and volume change with Ca content. The trend is linear with composition between 1 and 0.4 Ca apfu, but at about 0.4 Ca apfu a turnover is observed, with a sudden increase in the β angle, and a further decrease in the axial parameters, most apparent along the **a** axis, and in the cell volume ($V$).

Similar trends were found in diopside-enstatite (Tribaudino 2000; Tribaudino et al. 2005), and in $MnMgSi_2O_6$-$CaMgSi_2O_6$ pyroxenes (Arlt et al. 1998), for the Mg for Ca and Mn for Ca substitutions, respectively, and were all ascribed to the transformation from $C2/c$ to the $P2_1/c$ phase. We expect the $C2/c$ to $P2_1/c$ transition when a smaller cation, like Co here, substitutes Ca in the M2 site, or when cooling from high temperature reduces the apparent size of the cation in the M2 site (Arlt et al. 1998; Tribaudino et al. 2002).

The signature of the transition is, however, the presence of $h+k$ odd reflections, symmetry forbidden in $C2/c$ pyroxenes. Such reflections are best observed in single-crystal investigations, as they are present but quite weak in powder diffraction patterns. Single-crystal XRD refinements recently performed on pyroxenes between $CaCoSi_2O_6$ and $Ca_{0.4}Co_{1.6}Si_2O_6$, the $h+k$ odd reflections were not found, prompting for a $C2/c$ structure (Mantovani et al. 2013).

Synthesis of samples with lower Ca contents was attempted, but we did not manage to obtain single crystals large enough. Alternatively, the tiny crystals we synthesized were suitable for the observation with transmission electron microscopy: due to the high-scattering power of electrons, single-crystal electron diffraction patterns can be easily obtained from submicrometric areas.

As shown in Figure 5, selected area diffraction patterns taken on some flakes of composition $Ca_{0.3}Co_{1.7}Si_2O_6$, all revealed the presence of $h+k$ odd reflections, confirming that composition has a primitive lattice and assumingly a $P2_1/c$ symmetry. We can therefore divide the series by the different symmetry: Ca-richer samples with Ca between 1 and 0.4 apfu show a $C2/c$ symmetry that switches to $P2_1/c$ for lower Ca. This result was confirmed by subsequent careful analysis of powder diffraction patterns that revealed the presence of the weak $\bar{2}\bar{3}1$ reflection in $Ca_{0.3}Co_{1.7}Si_2O_6$ and $Ca_{0.2}Co_{1.8}Si_2O_6$ (Fig. 6).

## DISCUSSION

The above data show that at $P$ = 3 GPa along the $CaCoSi_2O_6$-$Co_2Si_2O_6$ series all the phases have the pyroxene structure, in contrast to room pressure. The same is true in Ca-Fe and Ca-Mg pyroxenes, but not in pyroxenes along the series $CaZnSi_2O_6$-$Zn_2Si_2O_6$ (Huber et al. 2012), which require higher pressure to stabilize the pyroxene phases.

As shown in Figure 3b there are several common features in the shape of the phase diagram for Ca vs. Fe, Mg and Co substitutions: (1) a large miscibility gap exists between Ca-rich and Ca-poor pyroxenes; (2) the gap is asymmetric, with much wider solubility in the Ca-richer side, whose symmetry is monoclinic $C2/c$; (3) on the Ca-poorer side of the join an orthopyroxene phase is present, with Ca up to a maximum content of 0.1 atoms per formula units (apfu); (4) an hypersolvus subsolidus field exists; and (5) monoclinic pyroxenes with a low-Ca content show a $P2_1/c$ space group.

The main difference between the three phase diagrams is the different solubility of Ca in the Ca-rich side of the series, whereas the solubility appears quite similar on the Ca-poorer orthopyroxene side.

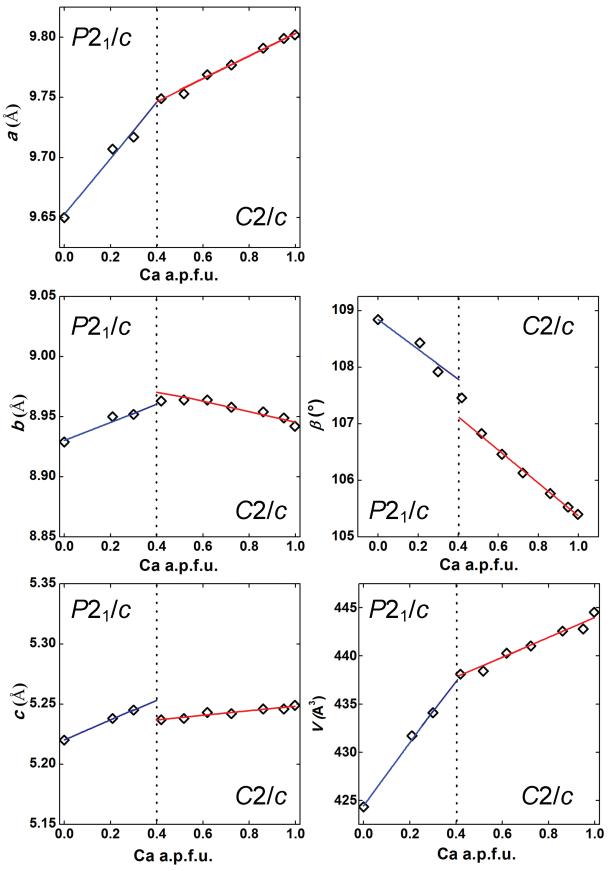


**FIGURE 4.** Cell parameters along the join $CaCoSi_2O_6$-$Co_2Si_2O_6$ in the *C*2/*c*, red, and *P*2$_1$/*c*, blue fields. (Color online.)

Such differences are due to a change in the size of the substituting cation, i.e., to an increase in the difference of the ionic radius with Ca, and provide a good example of the general principle that the extent of a solid solution depends on the difference in cation radius between the substituting cations. The difference in cation radius between Ca and Fe, Co, and Mg, is 22, 25.5, and 28%, respectively of the cation radius of Ca (Shannon 1976), and the solubility in the different series decreases with increasing difference in the cation radius.

Changes in space group along the series occur because Ca-poorer samples require a more deformed, less symmetric structure to accommodate smaller cations. This was observed in Mantovani et al. (2013) showing that the deformation parameter ΔM2 in *C*2/*c* structure increases with the decrease of Ca content up to a limiting value that triggers the transition. The difference between Ca-Mg, Ca-Fe, and Ca-Co here is in the composition at the transition from *C*2/*c* to *P*2$_1$/*c*, which was determined between 0.30 and 0.40 Ca apfu in Ca-Co and Ca-Fe pyroxenes and at about 0.60 Ca apfu, in Ca-Mg ones (Ohashi et al.1975; Newton et al. 1979; Tribaudino 2000; Tribaudino et al. 2005). This corresponds approximately to the turnover in volume vs. composition (Fig. 7), in agreement also with previous observation on $MnMgSi_2O_6$-$CaMnSi_2O_6$ pyroxenes (Arlt et al. 1998).

The volume changes in the *C*2/*c* Ca-richer pyroxenes can be modeled assuming that they are simple and only due to the

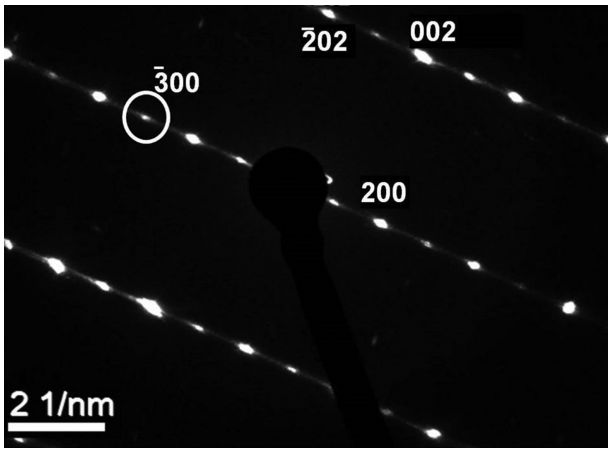


**FIGURE 5.** Selected-area electron diffraction pattern along [010] of $Ca_{0.3}Co_{1.7}Si_2O_6$. Note the presence of reflections *h*+*k* odd, violating the C lattice and of streaking along a*, interpreted as staking disorder, as in Tribaudino (2000).

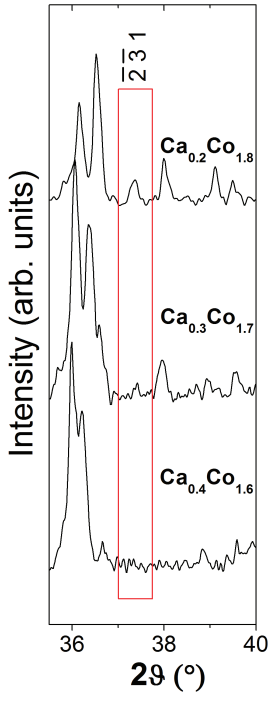


**FIGURE 6.** The evolution with composition of the *h*+*k* odd $\bar{2}3\bar{1}$ reflection between $Ca_{0.4}Co_{1.6}Si_2O_6$ and $Ca_{0.2}Co_{1.8}Si_2O_6$. (Color online.)

decreasing average size of the cation in the M2 site. The unit-cell volume can then be predicted as

$$V_x = V_{EM} - Z{\cdot}4/3\pi(R^3_{Ca} - R^3_{Fe,Co,Mg})(1 - X_{Ca})$$

where $V_x$ is the unit-cell volume for a given Ca content; $V_{EM}$ the volume of the Ca-rich end-member, i.e., diopside, hedenbergite, or $CaCoSi_2O_6$; *Z* the number of M2 sites in the unit cell (4 in *C*2/*c* and *P*2$_1$/*c*); and $R_{Ca}$ and $R_{Fe,Co,Mg}$ the ionic radii of divalent Ca and Fe, Co, and Mg. This trend predicts quite closely the

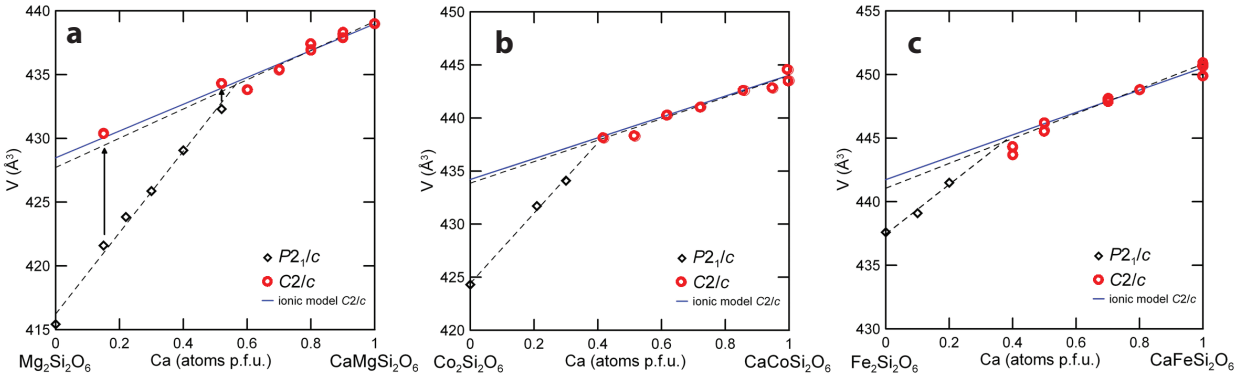


**FIGURE 7.** Cell volume vs. composition in Ca-Co, Ca-Mg, and Ca-Fe pyroxenes: the blue lines represent change in volume modeled by a "ionic model" (see text); red circles the experimental data for *C*2/*c*, room and extrapolated from high temperature (arrowed); and black diamond for $P2_1/c$ pyroxenes [Newton et al. (1979); Tribaudino (2000); Tribaudino et al. (2005) for Ca-Mg, Ohashi et al. (1975) for Ca-Fe pyroxenes]. Best fits for *C*2/*c* and $P2_1/c$ are dashed. (Color online.)

changes in volume with composition, which can be modeled as linear in the *C*2/*c* field (Fig. 7), up to the compositions close to the transition, where the observed volumes are lower than those predicted by the model.

While the above linear model is followed quite closely by Ca-richer *C*2/*c* clinopyroxenes, in the $P2_1/c$ field the cell volume is lower than predicted. We interpret the missing volume mostly as an effect of the *C*2/*c*–$P2_1/c$ transition. At high temperature the $P2_1/c$ pyroxenes undergo a displacive transition to *C*2/*c*; in Ca-Mg clinopyroxenes, the transition was observed at $T \sim 950$ and 550 °C in $Ca_{0.15}Mg_{1.85}Si_2O_6$ and $Ca_{0.52}Mg_{1.48}Si_2O_6$ pyroxenes, respectively (Tribaudino et al. 2002, 2003b). From an extrapolation of the volume of the *C*2/*c* pyroxenes above the transition temperature to room conditions, we obtain the volume that these compositions would have without the *P*–*C* transition. As shown in Figure 7 the volume plots very close to the linear *C*2/*c* trend obtained by the above "ionic" model.

To note, the volume–composition trend we observe in Ca-Fe, Ca-Mg, and Ca-Co pyroxenes could also be interpreted as non-ideal in a continuous solid solution. Here instead it is interpreted as ideal for *C*2/*c* and $P2_1/c$ pyroxenes, and the apparent deviation from non-ideality is due to a negative volume contribution for the phase transition. The composition at the transition can then be pinpointed at the turnover in the volume with composition trend, obtained by an extrapolation of the $P2_1/c$ volumes into the *C*2/*c* trend.

The transition in Ca-Mg pyroxenes is then determined at 0.58 Ca apfu, in agreement with previous TEM, Raman, and XRD observations (Tribaudino 2000; Tribaudino et al. 2005, 2012), and at about 0.39 Ca apfu for Ca-Co and 0.38 apfu for Ca-Fe pyroxenes, as supported by single-crystal X-ray diffraction results (Ohashi et al. 1975; Mantovani et al. 2013). A further result can be obtained along the series $CaMgSi_2O_6$-$MnMgSi_2O_6$, where Mg act as scaffolding cation in the M1 site, all Mn substitutes Ca in the M2 site, and the volume-composition trend shows that the transition occurs at 0.21 Ca apfu (Arlt and Armbruster 1997).

The average cation radius at the transition varies then between 0.88 Å for Ca-Mg, 0.86 Å for Ca-Fe and Ca-Mn, and 0.85 Å for Ca-Co pyroxenes, below, but not far from, the 0.89 Å critical cation radius estimated by an extrapolation of the $P2_1/c$–*C*2/*c* high-temperature transition temperatures to room temperature (Arlt and Angel 2000; Alvaro et al. 2011); it should be stressed however that the limited data set near the transition hinders careful determination of the critical composition.

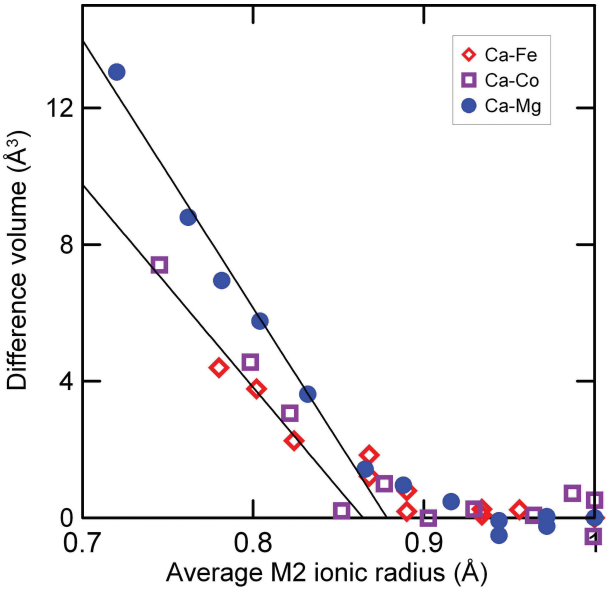


**FIGURE 8.** Difference with cation radius between experimental volume and that predicted by a "ionic model." Different best fit lines for Ca-Mg, and for Ca-Co and Ca-Fe pyroxenes are shown, calculated using only data from the $P2_1/c$ region. (Color online.)

A plot of the volume difference between the linear "ionic" model and the actual volume shows for the $P2_1/c$ pyroxenes a linear trend, with different slope and intercept for Ca-Mg and for Ca-Fe and Ca-Co pyroxenes (Fig. 8). The suggestion is that the *C*2/*c* phase is stabilized in Ca-Fe and Ca-Co pyroxenes.

Beyond ionic radius, a further contribution from the crystal field stabilization energy, which is present in Fe and Co pyrox-

ene, is therefore likely. An effect of the crystal field splitting was found by Arlt et al. (1998) in the high-pressure $P2_1/c$–$C2/c$ phase transition, comparing the transition pressure of $Mn^{2+}$ and $Cr^{2+}$ with that of clinoenstatite and clinoferrosilite. It was suggested that the effective ionic radii of M1 and M2 cations do not exclusively control the transition pressure: the HP $C2/c$ clinopyroxenes with $Cr^{2+}$ and $Fe^{2+}$ gain additional stabilization energy from crystal field effects.

## Implications

The rule of thumb for solid solutions, derived by investigations on metals (Hume-Rothery 1939) is that the difference in ionic radius of substituting cations of a given charge is the factor limiting the occurrence and extent of a solid solution. The rule was generalized by Kerrick and Darken (1975), stating that the difference in the molar volume of the end-members is the driving force. This is found here comparing Ca-Fe and Ca-Mg pyroxenes, where the solid solution is lower in the Ca-Mg and higher in the Ca-Fe series: in the two series the cation radius and the molar volume difference are higher and lower, respectively; pyroxenes in the Ca-Co series are in between. We see that the mere cation substitution explains only a part of the volume change through the solid solution: comparing clinoenstatite and diopside the deviation in the volume-composition for the phase transition in clinoenstatite is higher than that for the Ca-Mg substitution only (Fig. 7). Also, without the phase transition, the volume-composition behavior would be ideal. Alone, the difference in the molar volume between the end-members without the phase transition is similar in the three series, between 8 and 10 $Å^3$, and the final difference in the molar volume is due to the higher excess volume for the transition in Ca-Mg vs. Ca-Co and Ca-Fe (respectively, ~14, 10, and 5 $Å^3$). The different solid solution in the three series is therefore due to a different excess volume in the phase transition. It is likely that also for other thermodynamic variables the deviation in the thermodynamic behavior due to the phase transition is present: for instance Mg-richer $P2_1/c$ pyroxenes in the series diopside-enstatite show a marked deviation from the trend shown by $C2/c$ Ca-richer ones in the formation enthalpy (Newton et al. 1979). The obvious result is that when the phase transition is no more present (at about 1200 °C in the diopside-enstatite), but at much lower temperature in Fe-rich pyroxenes (Shimobayashi and Kitamura 1991; Arlt et al. 1998; Alvaro et al. 2011), the excess volume decreases significantly, and so the other thermodynamic excess parameters; the free energy of the solid solution becomes comparable or even lower than that of a mixture of Ca-richer and-poorer clinopyroxenes, and higher solid solution is possible.

This was observed already by Cameron and Papike (1981), on crystal chemical grounds: the much higher solid solution of pyroxenes at higher temperature could be explained by the presence of a $C2/c$ structure also in Fe-Mg-richer pyroxenes: in a $C2/c$ structure Ca enters more easily in solid solution than in the $P2_1/c$.

The change from $P2_1/c$ to $C2/c$ at high temperature occurs via a first-order transition (Smyth 1974; Tribaudino et al. 2002), and the volume changes suddenly at the critical transition point. Therefore, the transition temperature, the volume change before and after the transition should be well determined in modeling the end-member thermodynamics.

The implication is that the same should be done in modeling for petrologic calculations of any solid solution involving phase transitions.

In general therefore a miscibility gap, of a given extent, may develop either simply by the strain due to the cation substitution, within a series where all the end-members have the same structure, or for the combined effect of cation substitution and phase transition, like here in pyroxenes. In the latter case we have to consider the equilibria above and below the phase transition: the free energy of the solid solution should incorporate explicitly also the contribution from the phase transition.

A suggestion for further work in solid solution involving phase transitions would be to assess the energetic contributions due to the cation substitution alone and to phase transitions, where present. The purpose should be to define a model clarifying how the deformations due to these two mechanism compete. Also, from the petrologic point of view one should verify whether neglecting the effect of phase transitions in solid solutions may lead to incorrect extrapolation of the thermodynamic database outside the experimental conditions.

## Acknowledgments

The present study, and the companion paper by Mantovani et al. (2013), benefited from financial support from Italian PRIN 2010-2011 Grant 2010 EARRRZ_005; Ph.D. scholarship of Luciana Mantovani was paid within the MIUR "Progetto Giovani 2009" funding. Comment and suggestion by Gunther Redhammer and Gianluca Iezzi are gratefully acknowledged. Andrea Comelli and Luca Barchi are thanked for thin section preparation and SEM-EDS analyisis.

## References cited

Akimoto, S.I., Katsura, T., Syono, Y., Fujisawa, H., and Komada, E. (1965) Polymorphic transitions of pyroxenes $FeSiO_3$ and $CoSiO_3$ at high pressures and temperatures. Journal of Geophisical Research, 70, 5269–5278.

Alvaro, M., Camara, F., Domeneghetti, M.C., Nestola, F., and Tazzoli, V. (2011) H$T$ $P2_1/c$–$C2/c$ phase transition and kinetics of $Fe^{2+}$-Mg order-disorder of an Fe-poor pigeonite: Implications for the cooling history of ureilites. Contributions to Mineralogy and Petrology, 162, 599–613.

Arlt, T., and Angel, R.J. (2000) Displacive phase transitions in C-centred clinopyroxenes: Spodumene, $LiScSi_2O_6$ and ZnSiO. Physics and Chemistry of Minerals, 27, 719–731.

Arlt, T., and Armbruster, T. (1997) The temperature–dependent $P2_1/c$–$C2/c$ phase transition in the clinopyroxene kanoite $MnMg[Si_2O_6]$: A single crystal X-ray and optical study. European Journal of Mineralogy, 9, 953–964.

Arlt, T., Angel, R.J., Miletich, R., Armbruster, Th., and Tjerk, P. (1998) High-pressure $P2_1/c$–$C2/c$ phase transitions in clinopyroxenes: influence of cation size and electronic structure. American Mineralogist, 83, 1176–1181.

Bromiley, G.D., Keppler, H., McCammon, C., Bromiley, F.A., and Jacobsen, S.D. (2004) Hydrogen solubility and speciation in natural, gem-quality chromian diopside. American Mineralogist, 89, 941–949.

Burns, R.G. (1993) Mineralogical Applications of Crystal Field Theory. Cambridge University Press, U.K.

Cameron, M., and Papike, J.J. (1981) Structural and chemical variation in pyroxenes. American Mineralogist, 66, 1–50.

Domeneghetti, M.C., Molin, M., Stimpfl, M., and Tribaudino, M. (1995) Orthopyroxene from the Serra de Magé meteorite: Structure refinement and estimation of $C2/c$ pyroxene contributions to apparent *Pbca* diffraction violations. American Mineralogist, 80, 923–929.

Downs, R.T. (2003) Topology of the pyroxenes as a function of temperature, pressure, and composition as determined from the procrystal electron density. American Mineralogist, 88, 556–566.

Durand, G., Vilminot, S., Rabu, P., Derory, A., Lambour, J.P., and Ressouche, E. (1996) Synthesis, structure, and magnetic properties of $CaMSi_2O_6$ ($M$ = Co, Ni) compounds and their solid solutions. Journal of Solid State Chemistry, 124, 374–380.

Gasparik, T., and Lindsley, D.H. (1980) Phase equilibria at high pressure of pyroxenes containing monovalent and trivalent ions. In C.T. Prewitt, Ed., Pyroxenes, 7, p. 309–339. Reviews in Mineralogy and Geochemistry, Mineralogical Society of America, Chantilly, Virginia.

Ghose, S., Wan, C., and Okamura, F.P. (1987) Crystal structures of $CaNiSi_2O_6$ and $CaCoSi_2O_6$ and some crystal-chemical relations in $C2/c$ clinopyroxenes. American Mineralogist, 72, 375–381.

Huber, A.L., Heuss-Aßbichler, S., Fehr, K.T., and Bromiley, G.D. (2012) Petedunnite ($CaZnSi_2O_6$): Stability and phase relations in the system CaO-ZnO-$SiO_2$. American Mineralogist, 97, 739–749.

Hugh-Jones, D.A., Woodland, A.B., and Angel, R.J. (1994) The structure of high-pressure *C*2/*c* ferrosilite and crystal chemistry of high-pressure *C*2/*c* pyroxenes. American Mineralogist, 79, 1032–1041.

Hume-Rothery, W. (1939) The Structure of Metals and Alloys, Part III, p. 30–49. Chemical Publishing, Brooklyn, New York.

Jodlauk, S., Becker, P., Mydosh, J.A., Khomskii, D.I., Lorenz, T., Streltsov, S.V., Hezel, D.C., and Bohatý, L. (2007) Pyroxenes: a new class of multiferroics. Journal of Physics: Condensed Matter, 19, 432201.

Kerrick, D.M., and Darken, L.S. (1975) Statistical thermodynamic models for ideal oxide and silicate solid solutions, with application to plagioclase. Geochimica et Cosmochimica Acta, 39, 10, 1431–1442.

Larson, A.C., and Von Dreele, R.B. (1994) General Structure Analysis System (GSAS). Los Alamos National Laboratory Report LAUR 86-748.

Lindsley, D.H., and Munoz, J.L. (1969) Subsolidus relations along the join hedenbergite-ferrosilite. American Journal of Science, 267, 295–324.

Mantovani, L., Tribaudino, M., Mezzadri, F., Calestani, G., and Bromiley, G. (2013) The structure of $(Ca,Co)CoSi_2O_6$ pyroxenes and the Ca-$M^{2+}$ substitution in $(Ca,M^{2+})M^{2+}Si_2O_6$ pyroxenes ($M^{2+}$ = Co, Fe, Mg). American Mineralogist, 98, 1241–1252.

Mukhopadhyay, S., and Jacob, T. (1996) Phase equilibria in the system CaO-CoO-$SiO_2$ and Gibbs energies of formation of the quaternary oxides $CaCoSi_2O_6$, $Ca_2CoSi_2O_7$, and $CaCoSiO_4$. American Mineralogist, 81, 963–972.

Navrotsky, A., and Coons, W.E. (1976) Thermochemistry of some pyroxenes and related compounds. Geochimica et Cosmochimica Acta, 40, 1281–1288.

Newton, R.C., Charlu, T.V., Anderson, P.A.M., and Kleppa, O.J. (1979) Thermochemistry of synthetic clinopyroxenes on the join $CaMgSi_2O_6$-$Mg_2Si_2O_6$. Geochimica et Cosmochimica Acta, 43, 55–60.

Ohashi, Y., Burnham, C.W., and Finger, L.W. (1975) The effect of Ca-Fe substitution on the clinopyroxene crystal structure. American Mineralogist, 60, 423–434.

Redhammer, G., and Roth, G. (2004) Structural variation and crystal chemistry of $LiMe^{3+}Si_2O_6$ clinopyroxenes $Me^{3+}$ = Al, Ga, Cr, V, Fe, Sc, and In. Zeitschrift für Kristallographie–Crystalline Materials, 219, 5, 278–294.

Redhammer, G.J., Roth, G., Treutmann, W., Paulus, W., André, G., Pietzonka, C., and Amthauer, G. (2008) Magnetic ordering and spin structure in Ca-bearing clinopyroxenes $CaM^{2+}(Si, Ge)_2O_6$, M=Fe, Ni, Co, Mn. Journal of Solid State Chemistry, 181, 3163–3176.

Redhammer, G.J., Senyshyn, A., Tippelt, G., and Roth, G. (2011a) Magnetic spin structure of pyroxene-type $MnGeO_3$. Journal of Physics: Condensed Matter, 23, 254202.

Redhammer, G., Senyshyn, A., Tippelt, G., Pietzonka, C., Roth, G., and Amthauer, G. (2011b) Magnetic and nuclear structure and thermal expansion of orthorhombic and monoclinic polymorphs of $CoGeO_3$ pyroxene. Physics and Chemistry of Minerals, 37, 311–322.

Redhammer, G., Nestola, F., and Miletich, R. (2012) Synthetic $LiAlGe_2O_6$: The first pyroxene with $P2_1/n$ symmetry. American Mineralogist, 97, 1213–1218.

Sasaki, Y.T., Fujino, K., and Akimoto, S. (1982) Electron–density distribution of three orthopyroxenes, $Mg_2Si_2O_6$, $Co_2Si_2O_6$ and $Fe_2Si_2O_6$. Zeitschrift für Kristallographie, 158, 279–297.

Shannon, R. (1976) Revised effective ionic radii and systematic studies of interatomic distances in halides and chalcogenides. Acta Crystallographica, A32, 751–767.

Shimobayashi, N., and Kitamura, M. (1991) Phase transition in Ca-poor clinopyroxenes: a high-temperature transmission electron microscopic study. Physics Chemistry Minerals, 18, 153–160.

Smyth, J.R. (1974) The high temperature crystal chemistry of clinohypersthene. American Mineralogist, 59, 1061–1082.

Toby, B.H. (2001) EXPGUI, a graphical user interface for GSAS. Journal of Applied Crystallography, 34, 210–213.

Tribaudino, M. (2000) A transmission electron microscope investigation of the *C*2/*c*→*P*2$_1$/*c* phase transition in clinopyroxenes along the diopside-enstatite ($CaMgSi_2O_6$-$Mg_2Si_2O_6$) join. American Mineralogist, 85, 707–715.

Tribaudino, M., and Nestola, F. (2002) Average and local structure in $P2_1/c$ clinopyroxenes along the join diopside-enstatite ($CaMgSi_2O_6$-$Mg_2Si_2O_6$). European Journal of Mineralogy, 14, 549–555.

Tribaudino, M., Pasqual, D., Molin, G.M., and Secco, L. (2003a) Microtextures and crystal chemistry in $P2_1/c$ pigeonites. Mineralogy and Petrology, 77, 161–176.

Tribaudino, M., Nestola, F., Meneghini, C., and Bromiley, G.D. (2003b) The high-temperature $P2_1/c$–*C*2/*c* phase transition in Fe-free Ca-rich $P2_1/c$ clinopyroxenes. Physics and Chemistry of Minerals, 30, 527–535.

Tribaudino, M., Nestola, F., and Meneghini, C. (2005) Rietveld refinement of clinopyroxenes with intermediate Ca-content along the join diopside-enstatite. The Canadian Mineralogist, 43, 1411–1421.

Tribaudino, M., Mantovani, L., Bersani, D., and Lottici, P.P. (2012) Raman spectroscopy of $(Ca,Mg)MgSi_2O_6$ clinopyroxenes. American Mineralogist, 97, 1339–1347.

White, B.W., McCarthy, G.J., and Scheetz, B.E. (1971) Optical spectra of chromium, nickel, and cobalt-containing pyroxenes. American Mineralogist, 56, 72–89.

Yang, H., and Prewitt, C.T. (2000) Chain and layer silicates at high temperatures and pressures. In R.M. Hazen and R.T. Downs, Eds., High-Temperature and High-Pressure Crystal Chemistry, 41, p. 211–255. Reviews in Mineralogy and Geochemistry, Mineralogical Society of America, Chantilly, Virginia.

Manuscript received July 24, 2013
Manuscript accepted November 9, 2013
Manuscript handled by G. Diego Gatta